Are Changes in Global Precipitation Constrained by the Tropospheric Energy Budget?

F. HUGO LAMBERT*

Department of Geography, University of California, Berkeley, Berkeley, California

MYLES R. ALLEN

Department of Physics, University of Oxford, Oxford, United Kingdom

(Manuscript received 5 July 2007, in final form 24 July 2008)

ABSTRACT

A tropospheric energy budget argument is used to analyze twentieth-century precipitation changes. It is found that global and ocean-mean general circulation model (GCM) precipitation changes can be understood as being due to the competing direct and surface-temperature-dependent effects of external climate forcings. In agreement with previous work, precipitation is found to respond more strongly to anthropogenic and volcanic sulfate aerosol and solar forcing than to greenhouse gas and black carbon aerosol forcing per unit temperature. This is due to the significant direct effects of greenhouse gas and black carbon forcing. Given that the relative importance of different forcings may change in the twenty-first century, the ratio of global precipitation change to global temperature change may be quite different. Differences in GCM twentieth- and twenty-first-century values are tractable via the energy budget framework in some, but not all, models. Changes in land-mean precipitation, on the other hand, cannot be understood at all with the method used here, even if land–ocean heat transfer is considered. In conclusion, the tropospheric energy budget is a useful concept for understanding the precipitation response to different forcings but it does not fully explain precipitation changes even in the global mean.

1. Introduction

The conservation of energy, applied either to evaporation at the surface or to condensation in the troposphere, is a more severe constraint on increases in global precipitation than is the availability of atmospheric moisture (e.g., Mitchell et al. 1987; Allen and Ingram 2002; Yang et al. 2003). Hence, global precipitation rates increase at around 2% K^{-1} in general circulation models (GCMs), rather than following the 7.5% K^{-1} increase that would be predicted by the Clausius–Clapeyron equation (Held and Soden 2006). Recent work by Wentz et al. (2007) suggested that observed global precipitation may increase with the Clausius–Clapeyron equation. However, this is based on only 20 yr of data, neglects the effects of climatic natural variability, and

the different effects that different forcings may have on precipitation. The latter are the subject of this paper.

A problem may arise if we express precipitation changes in terms of temperature changes, because different radiative forcings on climate that produce the same change in global temperature can produce different changes in global precipitation due to the direct effects of some forcing agents on the troposphere. Granted, many authors have been interested specifically in the effect of increasing CO_2 on precipitation, rather than a combination of forcings. However, it is possible to separate the direct effect of forcings and their effect via global temperature change because of the time scales on which they operate. Doing so facilitates comparison between different models and between different forcings. Take, for example, the negative precipitation sensitivity of ECHAM4 to global warming when aerosol forcing is present (Roeckner et al. 1999; Liepert et al. 2004). It turns out that this is due to a large negative temperature-independent effect of forcings on precipitation and the relatively weak climate sensitivity of ECHAM4 global *temperatures*. It is not because precipitation scales negatively with temperature when

---

* Current affiliation: Met Office Hadley Centre, Exeter, United Kingdom.

Corresponding author address: F. Hugo Lambert, Met Office Hadley Centre, FitzRoy Rd., Exeter EX1 3PB, United Kingdom.
E-mail: hugo.lambert@metoffice.gov.uk

aerosols are present. The dependence of ECHAM4 precipitation on temperature is in fact fairly independent of the presence of aerosols (B. Liepert 2006, personal communication). The temperature-independent effect of forcing on precipitation is probably dominated by greenhouse gases, as we shall see below.

Energy conservation arguments work best for global precipitation. At smaller scales, changes in precipitation can be dominated by local processes. It may not be possible to write down changes in precipitation via a simple formula—particularly where advection of energy in or out of the region considered is important. For example, because zonal mean precipitation is dominated by changes in moisture convergence and divergence, precipitation changes take opposing signs at different latitudes. We must be careful, therefore, when applying energy budget constraints below global scale that our results are meaningful, such as for surface-based observed precipitation data only available over land.

The question for this paper is whether we can write down a simple model to help us understand the processes controlling global precipitation analogous to energy balance models used to understand global temperature change. We apply the argument of Mitchell et al. (1987) and Allen and Ingram (2002) that global precipitation changes are constrained by the perturbation energy budget of the troposphere to twentieth-century observed and modeled precipitation data. Using surface temperature and radiative forcing data, we attempt to reproduce precipitation changes via a linear regression model of the troposphere. We could equally well conserve energy at the surface (e.g., Boer 1993). However, the tropospheric argument allows us to contrast individual forcings transparently. We therefore make implicit assumptions about the surface energy and moisture budgets. Where these break down, our model cannot reproduce observed precipitation.

Our interest is not only in improving our physical understanding of precipitation change, but also in estimating the possible range of twenty-first-century precipitation more independently of GCMs. This is possible if the observed twentieth-century precipitation change can be expressed in terms of observed twentieth-century temperatures and forcings. We may then apply the observed fit to twenty-first-century forcing estimates (Nakicenovic et al. 2000) and a probabilistic forecast of twenty-first-century temperature made by, for example, Stott and Kettleborough (2002). [The future temperature trends derived by Stott and Kettleborough (2002) rely on the HadCM3 model, as well as observations.] Although some modern GCMs can adequately simulate forced changes in observed twentieth-century global-land precipitation (Lambert et al. 2005), their range of

twenty-first-century projections is not determined by our knowledge of observations.

Section 2 describes the observed and modeled data used, section 3 our method for expressing precipitation change via the tropospheric energy budget, section 4 our results, section 5 the possible effects of land–atmosphere coupling on land precipitation, and section 6 the differing responses of twentieth- and twenty-first-century GCM precipitation. We discuss our conclusions in section 7.

2. Observed data and model simulations

We consider gridded twentieth-century precipitation and temperature anomalies with respect to 1961–90. Global and ocean-only means are taken for each model dataset; land means are taken over the area sampled by precipitation observations for each model dataset and the observations. Hence, observations and model data are comparable over land. (Surface-based precipitation observations are unavailable over the oceans.) Forcing data are available as global means only.

a. Observed temperatures and precipitation

Observed precipitation data are taken from the Hulme dataset on a 2.5° latitude × 3.75° longitude grid for 1901–98 (Hulme 1992; New et al. 2000). The data are derived from surface-based precipitation gauges and are only available over land. During a given year, data are "masked" so that only grid boxes for which 7 of 12 months' worth of data are available are used. This is an arbitrary criterion that has little effect on our results. The global land-mean time series is plotted in Fig. 1c. Satellite and merged datasets that provide precipitation over the oceans are available, but none provides the length of record necessary for our analysis (Huffman et al. 1997; Xie and Arkin 1997; Wentz et al. 2007).

Observed temperatures are taken for the same period from version 3 of the Hadley Centre–Climate Reseach Unit global temperature anomalies dataset (HadCRUT3; Brohan et al. 2006). Spatial coverage is more complete than for the precipitation data. However, we remove data for which there are no corresponding precipitation observations for the sake of comparison. The global land-mean time series is plotted in Fig. 2c.

b. GCM temperatures, precipitation, and forcing

We use GCM data from nine fully coupled ocean–atmosphere models with sea ice and land surface schemes. Data for the National Center for Atmospheric Research's Community Climate System Model version 3 (NCAR CCSM3), the Geophysical Fluid Dynamics Laboratory's Coupled Climate Models versions 2.0
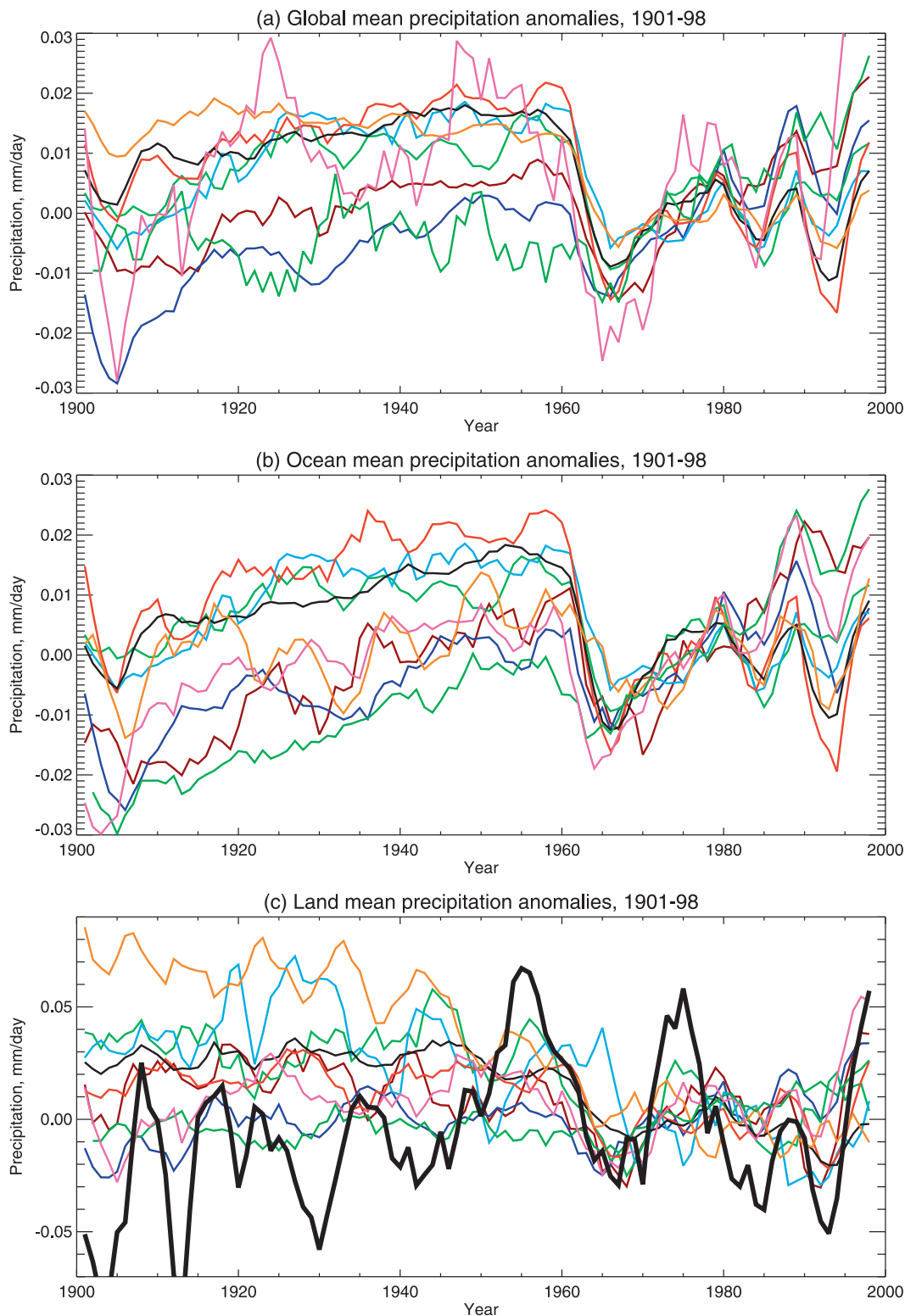
FIG. 1. The 5-yr running mean precipitation anomalies with respect to 1961–90 for 1901–98 averaged over all ensemble members for CCSM3, dark blue; GFDL0, pale green; GFDL1, pale blue; GISS (E-H), red; GISS (E-R), thin black; HadCM3, brown; MIROC, orange; MRI, dark green; PCM, pink; and the observations, thick black and land-mean only. (a) Global mean, (b) ocean mean, and (c) averaged over the land area sampled by the precipitation observations. Note the broader y-axis scale in (c).
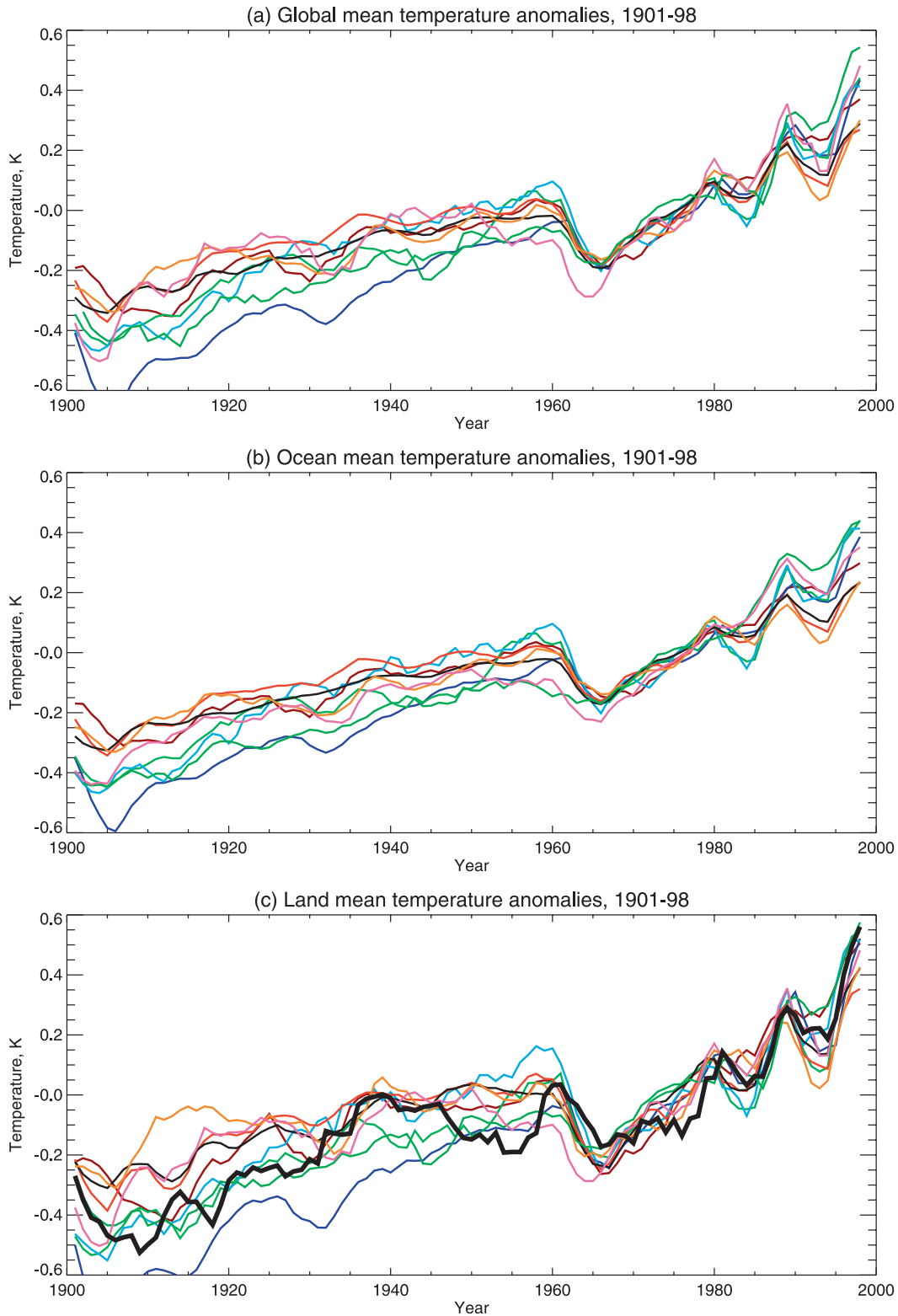
FIG. 2. The 5-yr running mean temperature anomalies with respect to 1961–90 for 1901–98 averaged over all ensemble members for CCSM3, dark blue; GFDL0, pale green; GFDL1, pale blue; GISS (E-H), red; GISS (E-R), thin black; HadCM3, brown; MIROC, orange; MRI, dark green; PCM, pink; and the observations, thick black and land-mean only. (a) Global mean, (b) ocean mean, and (c) averaged over the land area sampled by the precipitation observations.

TABLE 1. The number of ensemble members and the details of black carbon (BC), indirect sulfate (IS), solar, and volcanic SARF for each model. Where known, we have listed the SARF data origin.

Model	No. of ensemble members	BC	IS	Solar	Volcanic
CCSM3	5	Yes	Yes	L95[a]	Yes
GFDL0	3	Yes	No	L95	R00[b]
GFDL1	3	Yes	No	L95	R00
GISSH	5	Yes	M02[c]	L02[d]	HS01[e]
GISSR	9	Yes	M02	L02	HS01
HadCM3	4	No	Yes	Yes	Yes
MIROC	3	Yes	Yes	Yes	Yes
MRI	5	No	No	L95	HS93[f]
PCM	3	No	No	HS93	AKZ[g]

[a] L95 represents Lean et al. (1995).
[b] R00 represents Ramachandran et al. (2000).
[c] M02 represents Menon et al. (2002).
[d] L02 represents Lean et al. (2002).
[e] HS01 represents Hansen and Sato (2001).
[f] HS93 represents Hoyt and Schatten (1993).
[g] AKZ represents C. M. Ammann et al. (2005, unpublished manuscript).

(GFDL CM2.0; hereafter GFDL0) and 2.1 (CM2.1; hereafter GFDL1), the Goddard Institute for Space Studies (GISS) E-H and E-R coupled atmosphere–ocean models, the medium-resolution version of the Model for Interdisciplinary Research on Climate 3.2 (MIROC medres), the Meteorological Research Institute's coupled GCM model (MRI), and the NCAR Parallel Climate Model (PCM) were provided by the Intergovernmental Panel on Climate Change's Fourth Assessment Report (IPCC AR4) model output database portal (information online at https://esg.llnl.gov:8443/index.jsp; see the acknowledgments). Data for the HadCM3 model were provided by P. Stott at the U.K. Met Office (Gordon et al. 2000; Johns et al. 2003). Because the output is on a variety of different grids, model data are first interpolated onto the observed grid before masking and calculation of land means. For each model, an unforced control simulation and an ensemble of forced simulations driven with estimates of twentieth-century emissions are available. Precipitation time series are plotted in Fig. 1 and temperature time series in Fig. 2.

GCMs are forced by changing the concentrations of radiatively active species in the atmosphere, or, in the case of solar forcing, by changing the solar irradiance with time. The relative importance of different forcing agents can be most easily gauged by comparing the net downward radiative effect of each applied at the tropopause in watts per square meter. For each forcing, this is calculated by temporarily returning climate system temperatures below the tropopause to the unforced control state and measuring the net radiation at the tropopause. The quantity obtained is known as the stratospherically adjusted radiative forcing (SARF), as the stratosphere is allowed to come into equilibrium with applied forcing. By doing this at various points during the simulation, SARF time series can be calculated.

The precise nature of the SARF differs between models (see Table 1), but each is forced with a minimum of anthropogenic greenhouse gases (GHGs), the direct effect of anthropogenic tropospheric sulfate aerosols, stratospheric volcanic aerosols, and changes in solar irradiance. Some models are additionally forced with black carbon aerosols and the indirect effects of sulfate aerosols. These data were provided by D. Stone (2006, personal communication).

In addition to SARF data, we also have direct measurements of tropospheric "SARF absorption" derived from the MIROC Spectral Radiation-Transport Model for Aerosol Species (SPRINTARS) model (Takemura et al. 2006). SPRINTARS is an add-on to the MIROC model that provides a more comprehensive description of atmospheric aerosol transport and interaction with radiation. Importantly for us, SARF data were calculated at the tropopause as in the other GCMs, but also at the surface using the same method. The difference between the tropopause and surface values is the amount of SARF absorbed by the troposphere.

There is no division of aerosol effects by aerosol type in the SPRINTARS results. However, they assumed that all reflection is due to sulfate aerosol and that all direct absorption is due to black carbon (T. Nazawa 2007, personal communication). SARF and absorption time series are plotted in Fig. 3. These data were provided by T. Nazawa at the National Institute for Environmental Studies and T. Takemura at Kyushu University.

3. The energy budget of the troposphere

We now express the changes in global precipitation in terms of the perturbation energy balance of the troposphere, following the approach of Mitchell et al. (1987) and Allen and Ingram (2002). Because the troposphere has a small heat capacity, equivalent to only 2–3 m of ocean, we can assume that it is in equilibrium on time scales of a few years and longer. [The atmospheric radiative damping time scale is around 30 days; see James (1994).] Hence, changes in the tropospheric latent heating, $L\Delta P$, which accompany changes in precipitation, must be balanced by changes in radiative and sensible cooling, ΔR,

$$L\Delta P - \Delta R = 0, \tag{1}$$

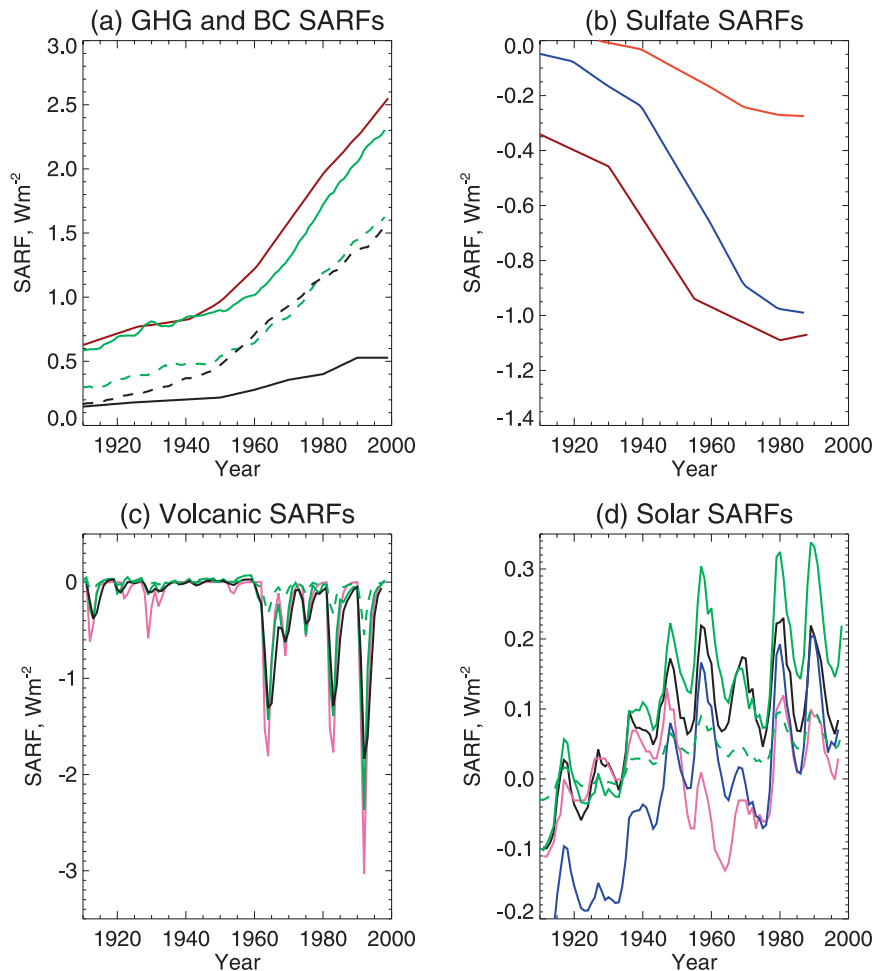and see Fig. 4. Linearizing ΔR, we write

FIG. 3. Values of SARF calculated from the twentieth-century simulations (solid lines) and SARF absorption in SPRINTARS (dashed lines). (a) GHG SARF in HadCM3 (solid brown) and MIROC SPRINTARS (solid green). The GHG SARF in other models is very similar (not shown). GHG absorption in SPRINTARS (dashed green). BC SARF in the GISS models (solid black). BC absorption in SPRINTARS (dashed black). (b) Total sulfate aerosol SARF, both direct and indirect, in HadCM3 (solid brown) and other models (dark blue). Direct sulfate aerosol SARF in the GFDL models (solid red). (c) Volcanic SARF in the GISS models derived from Hansen and Sato (2001) (solid black), in PCM derived from C. M. Ammann et al. (2005, unpublished manuscript) (solid pink), and in SPRINTARS derived from Sato et al. (1993) (solid green). Volcanic absorption in SPRINTARS (dashed green). (d) Solar SARF in the GISS models derived from Lean et al. (2002) (solid black); in PCM derived from Hoyt and Schatten (1993) (solid pink); and estimated by D. Stone from Lean et al. (1995) for GFDL, MRI, and CCSM3 (dark blue); as well as in SPRINTARS derived from Lean et al. (1995). Solar SARF absorption in SPRINTARS (dashed green).

$$L\Delta P \simeq k_T \Delta T + \Delta R_C + \Delta R_S, \qquad (2)$$

where positive $k_T \Delta T$ represents the net increases in radiative and sensible cooling due to changes in tropospheric temperature, positive ΔR_C represents the increases in net radiative cooling due to changes in tropospheric absorbing species concentration, and positive ΔR_S represents the net increases in cooling due to

changes in the net solar shortwave at the tropopause. (It is important to realize that ΔR_S is not simply the negative of the change in the absorbed insolation; see below.) Both ΔR_C and ΔR_S are taken to be independent of the surface temperature change. Hence, the effects of SARF on precipitation are divided into surface-temperature-dependent and -independent effects. Since the evolution of the former depends on the heat capacity
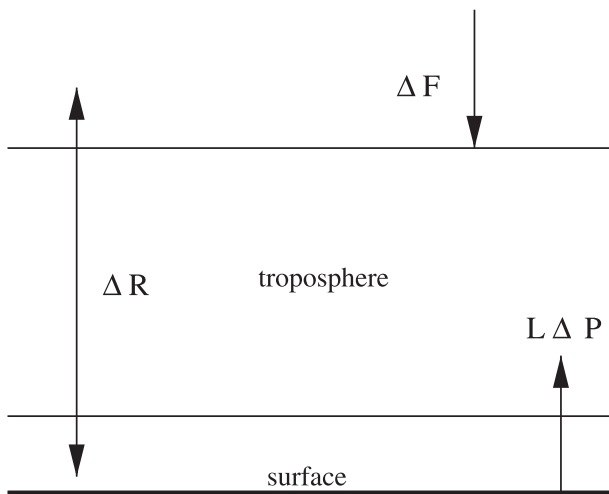
FIG. 4. A schematic energy budget diagram of the global troposphere. Because the heat capacity of the troposphere is small, we can assume that it is in equilibrium on climatological time scales. Hence, changes in latent heating, $L\Delta P$, must be balanced by changes in radiative and sensible heating, ΔR. Producing the increase in tropospheric temperature that generates an increase in precipitation requires the application of a SARF, ΔF. A ΔF that causes direct tropospheric heating independent of $L\Delta P$ produces a smaller change in precipitation because a smaller change in ΔT is needed to produce ΔR.

of the climate system, particularly the ocean mixed layer, but the latter are effectively instantaneous, separation by time scale is possible if some SARF components are applied rapidly, as is the case for volcanoes. Here, ΔT refers to surface temperatures, as observed data are available for the entire twentieth century. This may be problematic, as we rely on the ratio of tropospheric temperature change to surface temperature change being constant (see section 3b).

Consider an increase in global precipitation, ΔP, that accompanies an increase in global surface temperature, ΔT. Increasing ΔT increases the tropospheric temperature and cooling (primarily radiative). There are accompanying increases in solar shortwave absorption by water vapor as the water vapor concentration increases, and there may be significant temperature-dependent cloud feedbacks. The net tropospheric cooling from all these factors determines the total possible increase in latent heating, $L\Delta P$. To produce the increase in ΔT, however, we must first introduce a SARF, ΔF, via an external agent that affects climate. Doing so can produce further changes in the precipitation that are independent of temperature.

We could increase the net solar shortwave input into the climate system by, for example, increasing the solar irradiance or reducing the concentration of the stratospheric volcanic aerosols. The increase in solar irradi-

ance is absorbed primarily at the surface, causing an increase in surface temperature, ΔT, that is transmitted to the troposphere by latent, sensible, and radiative fluxes, as above. The resulting warmer troposphere cools at a higher rate, $k_T\Delta T$, chiefly due to radiation, and allows an increase in precipitation. Because some of the increase in solar irradiance is directly absorbed by the troposphere, we could also see a direct effect that reduces precipitation. However, idealized model experiments suggest that the atmosphere largely compensates for direct solar absorption by tropospheric warming that causes the emission of longwave radiation almost independent of changes in ΔT (Lambert and Faull 2007). This is termed tropospheric adjustment, and was originally shown for aerosol forcing (Rotstayn and Penner 2001). It is the reason why ΔR_S is not simply equal to the negative of the change in insolation absorbed by the troposphere. Allowing for tropospheric and rapid surface adjustment to occur before calculating the radiative forcing yields what we will call the tropospherically adjusted radiative forcing (TARF; see also Shine et al. 2003). If it was possible to calculate the amount of TARF absorbed, then we would expect this to be equal to ΔR_S. Estimation is possible for idealized GCM experiments using the method of Gregory et al. (2004), but where there are time variations in SARF, as in our experiments, this is not possible. In summary, we expect $\Delta R_S < 0$, opposing positive $k_T\Delta T$, and the increase in precipitation, but it should be small.

Forcing the climate system with an equivalent ΔF by increasing the concentration of atmospheric CO_2 produces a similar increase in ΔT and, hence, a similar increase in $k_T\Delta T$. However, adding CO_2 also increases the opacity of the atmosphere to infrared longwave radiation independent of temperature change. This causes longwave emission to space to originate from higher, colder levels, reducing the tropospheric radiative cooling. Tropospheric emission to the surface, meanwhile, increases, as radiation is emitted from lower, warmer levels. The effect on the emission to space dominates, because the change in emission altitude at the surface is relatively small because the relevant longwave emission regions are already quite saturated. This means that $\Delta R_C < 0$. Previous work suggests that the effect will be significant and will oppose positive $k_T\Delta T$ and reduce $L\Delta P$ (Mitchell et al. 1987; Allen and Ingram 2002; Yang et al. 2003; Lambert and Faull 2007). As for ΔR_S, there is evidence that tropospheric adjustment partially counters ΔT independent absorption due to GHGs (Gregory and Webb 2008). The adjustment occurs through changes in clouds. It is considerably smaller than in the solar case, however. Hence, we expect GHG SARFs that produce the same increase in ΔT as SARFs

that affect insolation to produce smaller increases in precipitation.

a. A regression model for global precipitation

To build a simple model compatible with the available data, we make further approximations for ΔR_C and ΔR_S that are linear in SARF. This is sensible in most cases, because SARF is the net radiative flux across the tropopause and a major component of ΔR. First, we write $\Delta R_C \simeq \beta_C \Delta F_C$, where ΔF_C is the SARF at the tropopause due to changes in the concentrations of atmospheric absorbing species and β_C is a constant to be determined. The SARFs that we consider to be part of ΔF_C are those that are simulated by the GCMs for which we have data. We treat GHGs, which unambiguously affect climate by absorbing longwave radiation, as composing the bulk of ΔF_C. We also include black carbon aerosols, which force climate by absorbing shortwave radiation (Haywood et al. 1997) and which may show a temperature-independent effect that reduces precipitation.

Similarly, we write $\Delta R_S \simeq \beta_S \Delta F_S$, where ΔF_S is the shortwave SARF due to changes in solar irradiance and reflecting aerosol concentration, and β_S is a constant to be determined. The relevant aerosol SARFs simulated by our models are changes in volcanic stratospheric aerosols, which very largely reflect shortwave radiation alone, and tropospheric sulfate aerosols, which reflect solar radiation by their direct and indirect effects, but may also be a source of longwave heating in the troposphere (Ramanathan et al. 2001).

Applying these substitutions in Eq. (2), we obtain

$$L\Delta P \simeq k_T \Delta T + \beta_C \Delta F_C + \beta_S \Delta F_S. \qquad (3)$$

b. Expected behavior of the regression model

If precipitation is to increase with GHG-driven global warming, then we expect k_T to be positive and for $k_T \Delta T$ to be large enough to outweigh negative $\beta_C \Delta F_C$. How constant should k_T be across models? Under global warming, current GCMs tend to retain an atmospheric temperature profile that is quite close to the moist-adiabatic lapse rate. Nevertheless, there is a spread in the temperature and closely coupled moisture profiles that produces a combined lapse rate–water vapor feedback range of around 1.0 ± 0.2 W m^{-2} K^{-1} at the tropopause across IPCC AR4 models (Soden and Held 2006). (The temperature change refers to the surface temperature change, as in our work. Errors are taken as two standard deviations, approximating 5%–95% confidence limits.) In addition, k_T depends on flux changes at the surface that have not been quantified. We might

expect them to be smaller because saturation in the relevant longwave emission bands near the surface will tend to reduce the effect of changes in atmospheric temperature profiles aloft. However, differences in GCM radiation code have been shown to produce considerably larger ranges in radiative fluxes at the surface than at the tropopause in response to prescribed changes in water vapor concentration (Collins et al. 2006). There is also no reason to expect the surface effect to be of the opposite sign as the tropopause effect, as it is for the temperature-independent effect of changing GHG concentration.

Soden and Held (2006) also describe large intermodel differences in cloud and albedo feedbacks. The most important differences are in reflected shortwave radiation, but these have only a secondary effect on the tropospheric energy budget because most of this energy is not absorbed by the troposphere. Therefore, although the reflection of shortwave radiation does influence ΔT and hence ΔP, it does not affect k_T. There are also longwave cloud feedbacks that do affect the tropospheric energy absorption. Their range of radiative effects at the tropopause is fairly small [e.g., -0.15 ± 0.3 W m^{-2} K^{-1} for nine AR4 GCMs from Webb et al. (2006)]. Their range of effects at the surface has not been quantified, however.

Adding the tropopause clear-sky and longwave cloud feedback ranges gives a total expected range for global k_T of about 0.4 W m^{-2} K^{-1}. This must be considered a minimum value, as differences at the surface also contribute.

Over land, we know that changes in surface humidity controlled by soil moisture can affect the local tropospheric energy budget by suppressing the dynamical processes that produce precipitation (Schär et al. 1999; Koster et al. 2004). This does not necessarily affect the mean land precipitation, as precipitation may simply fall elsewhere. However, if such processes do change precipitation over large enough land areas, then k_T may not be a constant, and treating precipitation as linear in temperature may be inappropriate.

Naïvely, we might expect β_S to be the negative of the fraction of the applied shortwave SARF absorbed in the troposphere. However, there should also be a positive tropospheric adjustment contribution from rapid tropospheric warming due to the emission of longwave radiation almost independent of warming at the surface, as discussed above. Lambert and Faull (2007) found that this positive contribution produced β_S that is consistent with zero in two slab (thermodynamic mixed-layer ocean) GCMs for solar forcing. Because on climatological time scales this occurs instantaneously, it is best considered part of β_S. Clearly, the positive contribution cannot be larger than the SARF absorbed, so β_S should be consistent with $-1 < \beta_S < 0$.

We expect β_C to be negative, but not less than -1. Longwave SARF contributes $-1 \times \Delta F_C$ to the tropospheric energy budget at the tropopause by definition. It also contributes a smaller, positive flux at the bottom of the atmosphere, increasing β_C (e.g., Goody and Yung 1989). There may be some tropospheric adjustment, as described by Gregory and Webb (2008), but we expect the effect on latent heat to dominate.

c. Additional problems

Above, we noted that using surface temperature change to provide ΔT introduces a spread in our estimates of k_T across models, because changes in the tropospheric lapse rate produce different changes in the tropospheric temperatures in different models. We also assume that k_T is the same for different SARFs. In addition to differences in the lapse rate, differences in the spatial pattern of the surface temperature response to different SARFs could produce different k_T. However, in the idealized experiments of Lambert and Faull (2007), k_T was consistent for CO_2 and solar SARF. We will also test the consistency of k_T for forced and unforced precipitation changes. Energy is conserved in all of these cases, but it may not be possible to fit a simple linear equation for precipitation change like Eq. (3), if coefficients are not similar enough across SARFs.

Black carbon aerosols can cause two further difficulties for our method. First, black carbon aerosol SARF is not always well related to tropospheric SARF absorption, especially over dark surfaces. We can circumvent this problem by directly calculating the tropospheric SARF absorption from the MIROC SPRINTARS data. Second, it is uncertain what fraction of black carbon aerosol absorption is compensated for by a reduction in latent heating, compared with greenhouse gas absorption. (Recall that solar SARF absorption is largely compensated for by the emission of tropospheric longwave radiation, rather than a reduction in latent heating.) Hence, combining the two types of SARF into ΔF_C may be inappropriate without first scaling the black carbon SARF. Idealized GCM experiments comparing the direct effects on precipitation of GHG and black carbon forcing are scarce. However, the work of Roberts and Jones (2004) suggests that the direct effect of black carbon on precipitation is very approximately 25% larger per unit SARF. In our analysis, we investigate the sensitivity of our results to applying this scaling. Because GHG and black carbon SARF are well correlated during the twentieth century (Fig. 3), introducing a separate black carbon regressor is not a good idea.

We now write alternative formulations for ΔR_C and ΔR_S based on tropospheric absorption. Here, $\Delta R_C \simeq$ $\beta_{AC}\Delta A_C$, where ΔA_C is the tropospheric GHG and black carbon SARF absorption calculated from the MIROC SPRINTARS model and β_{AC} is a constant to be determined. Similarly, $\Delta R_S \simeq \beta_{AS}\Delta A_S$, where ΔA_S is tropospheric shortwave absorption due to changes in solar irradiance and sulfate aerosol concentration and β_{AS} is a constant to be determined. Both β_{AC} and β_{AS} have the same numerical limits on them as β_C and β_S because the latter assume that SARF was greater than or equal to tropospheric absorption of SARF.

Equation (2) now becomes

$$L\Delta P \simeq k_T\Delta T + \beta_{AC}\Delta A_C + \beta_{AS}\Delta A_S. \qquad (4)$$

Compared to Eq. (3), Eq. (4) has the advantage that temperature-independent changes in precipitation are directly related to the SARF absorbed by the troposphere. It has the disadvantage that we only have absorption data for the MIROC model.

d. Application to observed and GCM data

Ordinary least squares (OLS) regression is used to estimate values of k_T, β_C, and β_S in Eq. (3), from 5-yr mean observed and GCM temperatures and precipitation, and the GCM SARF data; k_T, β_{AC}, and β_{AS} are estimated similarly in Eq. (4), except using the SPRINTARS SARF absorption data rather than SARF data. We use 5-yr means because the most predictable response in twentieth-century global-land precipitation occurs over 5–10-yr time scales (Lambert et al. 2004). This is most probably because time variations in the SARF series are dominated by these time scales.

We treat noise in $L\Delta P$ as white and as being due to internal climate variability alone. As a result, our analysis will tend to underestimate the regression parameter ranges for observations, as we neglect measurement errors. We calculate the noise variance from unforced control run GCM data. Where unforced temperature and precipitation data are positively correlated, as they are globally and over the ocean, we include only the component of precipitation variability that is uncorrelated with temperature in the noise variance. We do this because the correlated variability in the twentieth-century runs contains information that partially determines k_T. Of course, the relationships between forced temperature and precipitation and unforced temperature and precipitation may not be the same, due to differences in the forced and unforced surface temperature patterns as well as the forced and unforced precipitation patterns (Douville et al. 2006). There is no way to distinguish between these in the observations, however. We calculate k_T for the unforced control runs as a check. Introducing autocorrelation into

TABLE 2. Regression coefficients for global, ocean-only, and land sampled from observations only for 5-yr means when SARF data are used. In each case, k_T is calculated for the control run, and the temperature-dependent component of the precipitation variability is removed where k_T is significant at the 10% level and the correlation between $L\Delta P$ and T, $\rho(L\Delta P, T)$, is positive. Values of k_T, β_C, and β_S and their confidence limits are then given for the forced ensemble means for 1913–97. The F-test P value is quoted as a consistency check on residual variance. Values in boldface are significant at the 10% level.

	CCSM3	GFDL0	GFDL1	GISSH	GISSR	HadCM3	MIROC	MRI	PCM
Global									
control									
k_T (W m^{-2} K^{-1})	1.16	1.50	1.32	2.07	1.11	1.60	0.68	1.92	1.24
10%–90%	0.18	0.20	0.19	0.37	0.48	0.10	0.19	0.38	0.34
$\rho(L\Delta P, T)$	0.75	0.79	0.78	0.74	0.38	0.82	0.52	0.76	0.64
Res	0.01	0.02	0.01	0.01	0.01	0.01	0.01	0.01	0.01
ALL									
k_T (W m^{-2} K^{-1})	**0.91**	**1.68**	**1.54**	**1.78**	**1.59**	**1.97**	**0.84**	**1.87**	**1.92**
10%–90%	**0.32**	**0.49**	**0.34**	**0.57**	**0.41**	**0.33**	**0.48**	**0.36**	**0.35**
β_C	**0.17**	**−0.40**	**−0.48**	**−0.24**	**−0.32**	**−0.24**	**−0.25**	−0.11	−0.14
10%–90%	**0.14**	**0.14**	**0.10**	**0.19**	**0.14**	**0.13**	**0.15**	0.14	0.14
β_S	**0.33**	0.16	−0.06	**0.35**	**0.23**	0.07	**0.26**	0.17	**0.33**
10%–90%	**0.11**	0.17	0.16	**0.19**	**0.12**	0.08	**0.13**	0.10	**0.12**
F-test	1.00	**0.33**	**0.50**	0.91	0.95	**0.60**	0.97	1.00	**0.71**
Ocean									
control									
k_T (W m^{-2} K^{-1})	2.10	2.29	3.27	2.13	2.46	3.00	3.78	2.48	2.07
10%–90%	0.22	0.31	0.36	0.43	0.55	0.21	0.36	0.54	0.42
$\rho(L\Delta P, T)$	0.85	0.78	0.84	0.70	0.62	0.80	0.87	0.72	0.75
Res	0.01	0.04	0.04	0.02	0.01	0.02	0.02	0.02	0.01
ALL									
k_T (W m^{-2} K^{-1})	**1.52**	**1.68**	**1.54**	**2.49**	**1.85**	**3.11**	**2.90**	**2.16**	**2.45**
10%–90%	**0.32**	**0.74**	**0.59**	**0.68**	**0.46**	**0.54**	**0.87**	**0.50**	**0.42**
β_C	**−0.17**	**−0.40**	**−0.48**	**−0.33**	**−0.19**	**−0.28**	**−0.58**	−0.16	**−0.37**
10%–90%	**0.12**	**0.21**	**0.18**	**0.20**	**0.14**	**0.18**	**0.23**	0.20	**0.16**
β_S	0.06	0.16	−0.06	**0.35**	**0.36**	0.02	−0.20	0.10	0.14
10%–90%	0.09	0.26	0.27	**0.19**	**0.12**	0.12	0.20	0.13	0.14
F test	1.00	0.02	0.01	1.00	1.00	0.93	**0.29**	0.02	**0.73**
Land (observed mask)									
control									
k_T (W m^{-2} K^{-1})	0.30	−0.39	−1.98	1.41	−0.62	−1.41	−4.26	−0.16	−0.25
10%–90%	0.29	0.85	1.11	1.21	1.07	0.65	0.92	1.24	1.30
$\rho(L\Delta P, T)$	0.18	−0.08	−0.31	0.22	−0.11	−0.21	−0.65	−0.03	−0.05
Res	0.13	0.36	0.67	0.11	0.10	0.38	0.26	0.14	0.19
ALL									
k_T (W m^{-2} K^{-1})	−0.24	1.45	0.36	0.88	**1.16**	1.00	−0.19	0.97	0.92
10%–90%	0.81	2.06	2.24	1.79	**1.00**	1.42	3.00	1.05	1.45
β_C	**0.88**	−0.67	**−1.24**	−0.14	**−0.63**	−0.49	−0.42	−0.06	0.24
10%–90%	**0.43**	0.68	**0.79**	0.73	**0.43**	0.69	1.07	0.45	0.60
β_S	**1.02**	0.40	−0.91	0.48	0.18	0.12	1.04	0.14	**1.04**
10%–90%	**0.38**	0.90	1.27	0.77	0.42	0.48	1.12	0.37	**0.65**
F test	0.95	**0.41**	**0.69**	**0.11**	0.54	0.85	0.36	0.32	0.71

the noise model makes a negligible difference in each case, and will not be discussed further.

4. Regression results

We now present regression results for 5-yr mean precipitation, temperature, and SARF and SARF absorption for 1913–97. We begin by using the SARF data for individual models rather than the MIROC SPRINTARS SARF absorption data. We scale black carbon SARF by 1.25, as suggested by the findings of Roberts and Jones (2004).

a. GCM global-mean precipitation using SARF data

We find Eq. (3) to be a good model of global precipitation for 1913–97 in most of the nine GCMs. At the 10%–90% confidence level, k_T is positive and significant in all cases, and β_C is negative and significant in five cases; see Table 2. The value of β_S is small and positive in general and significant in five cases. Residual variance

is consistent with unforced variability simulated by the same GCM only in GFDL0, GFDL1, MIROC, and PCM. Unforced k_T is consistent with 1913–97 k_T apart from for PCM. The unforced precipitation and temperature have correlation coefficients of $\rho > 0.6$ in all models apart from in MIROC and GISS (E-R). Calculating the mean across the nine forced models, and giving equal weight to each model, we find $k_T = 1.56 \pm 0.19$ W m^{-2} K^{-1}, $\beta_C = -0.23 \pm 0.07$, and $\beta_S = 0.23 \pm 0.06$. The F-test P value is 1.00, indicating that the residual variance is too large when compared to a cross-model estimate of unforced variability. Nevertheless, the agreement looks excellent; see Fig. 5a. Removing the factor of 1.25 scaling for the black carbon aerosol SARF changes these regression results by < 0.03 in all cases (not shown). Further varying the black carbon scaling factor by as much as an order of magnitude does not produce differences significant at the 10%–90% level. It is also reassuring that k_T for HadCM3 is consistent with that for idealized experiments with the HadSM3 slab model found by Lambert and Faull (2007), as HadSM3 has the same atmospheric component as HadCM3. (Our HadCM3 β_L is also consistent with their HadSM3 $\Delta R_A = \beta_L \Delta F_L$ although their range of uncertainty is large.)

In different models k_T is different. This is not surprising, given that the feedbacks important to the tropospheric energy budget are also different (see section 3b). However, values of 1913–97 k_T plotted against the control k_T for the same model, more or less, lie on the line $y = x$, as we would expect if the regression model is reasonably robust (Fig. 6). Assuming that control k_T reliably describes the forced k_T, we can try imposing the values of control k_T on our 1913–97 regression, and calculating β_C and β_S alone. Values are consistent with the full regression in all but a few cases, but uncertainty ranges are somewhat reduced (Table 3). Interestingly, β_S is significant and positive in eight cases.

Positive β_S is a common theme in our results, and is contrary to our physical understanding. It may be an artifact of regression that part of the temperature-dependent response to precipitation is being fitted to the solar and sulfate aerosol shortwave SARF changes. This explanation may still hold, even though specifying the control k_T also produces significant positive values of β_S because forced and unforced precipitation changes may not be identical. Alternatively, there may be physical processes controlling the interaction between the precipitation and shortwave SARFs that we do not understand. For instance, if anticorrelated components of ΔF_S have quite different negative values of β_S, then the total β_S could come out as positive. We cannot test this with our data, however, because anthropogenic

sulfate SARF is strongly anticorrelated with solar and GHG SARFs, making the introduction of separate regressors impractical. Another possibility is that positive *longwave* SARF due to volcanic aerosol dominates β_S (W. Ingram 2008, personal communication). Although the longwave SARF due to volcanoes is small, it could cause positive β_S since we expect β_S due to shortwave absorption to be close to zero.

b. GCM ocean-mean precipitation using SARF data

Including only data over the oceans, we again find that Eq. (3) is a good model of the mean precipitation change. Here, k_T is positive and significant in all cases, β_C is negative and significant apart from for MRI, and β_S is significant and positive in GISS (E-H) and (E-R); see Table 2. In some cases, k_T is larger than for global means. Individual parameter values are less well constrained than for global means, but the general picture is the same. Values of unforced k_T are consistent with 1913–97 k_T, apart from for CCSM3 and GFDL1, and control precipitation–temperature correlations are > 0.6 in all cases. Taking the mean across all nine models, we find $k_T = 2.02 \pm 0.30$ W m^{-2} K^{-1}, $\beta_C = -0.29 \pm 0.10$, and $\beta_S = 0.15 \pm 0.09$. The F-test P value is 0.89, which is marginally consistent with the unforced GCM variability. Again, the fit is convincing (Fig. 5b).

c. Mean precipitation over the observed land area using SARF data

Global-mean precipitation time series resemble global-mean temperature time series, and ocean-mean precipitation time series resemble ocean-mean temperature time series (cf. Figs. 1 and 2). Over land, however, the situation is different. While the land-mean temperature behaves similarly to the global and ocean-mean temperature, the land-mean precipitation time series are not similar to the global and ocean-mean precipitation. The difference is reflected by our regression model, which fails to capture land precipitation change in most of the models. GISS E-R, and, to some extent, MRI are the exceptions (Table 2).

What if we allow for the advection of energy between the land and ocean atmospheres? Introducing a regression term into Eq. (3) proportional to the land–ocean energy transport is entirely unhelpful in the GFDL0, GFDL1, GISS (E-R), MIROC, and MRI models, for which we have heat flux data.

Taking the nine-model mean, however, improves things; see Fig. 5c. This appears to suggest that, although land precipitation is not controlled by the energy budget in most of the GCMs, whatever is controlling the precipitation produces different results in each case. When the GCM results are averaged together, an underlying
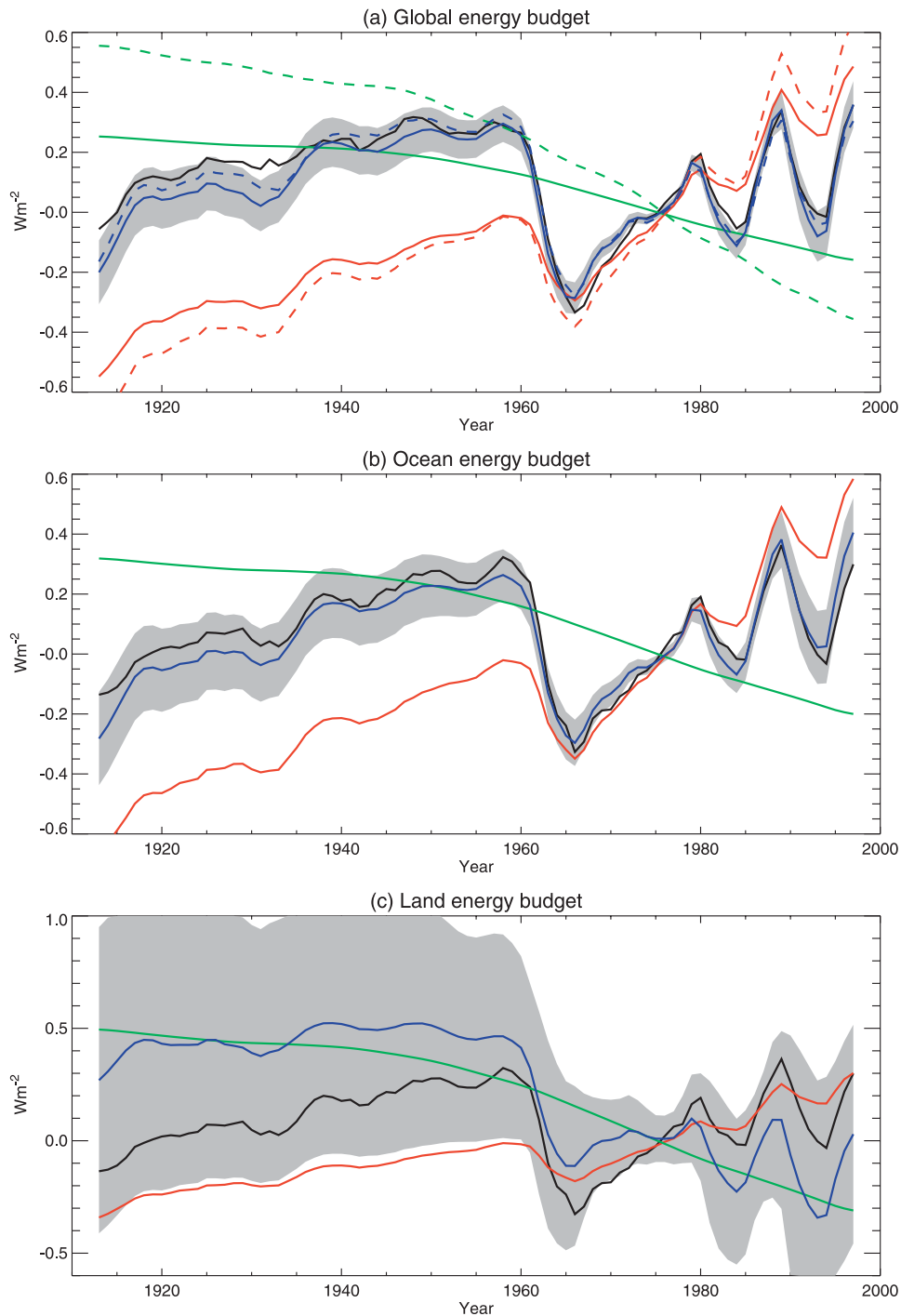
FIG. 5. The 5-yr running mean components of the perturbation tropospheric energy budget for 1913–97 averaged across all model ensemble members, and giving equal weight to each model. The solid lines are $L\Delta P$, black; $k_T\Delta T$, red; $\beta_C\Delta F_C$, green; and the best-fit reconstruction of $L\Delta P$ from regression (blue) where the SARF data and Eq. (3) are used. Here, $\beta_S\Delta F_S$ is not shown because it is small or positive, which conflicts with our physical understanding of the troposphere, in each case. The gray plume represents a 10%–90% confidence interval, which is smaller during 1961–90 because this is the period against which anomalies are calculated. (a) Global mean, (b) ocean mean, and (c) averaged over the land area sampled by the precipitation observations. The dashed lines in (a) represent $k_T\Delta T$ (red), $\beta_{AC}\Delta A_C$ (green), and the best-fit reconstruction (blue) where SARF absorption data and Eq. (4) are used.
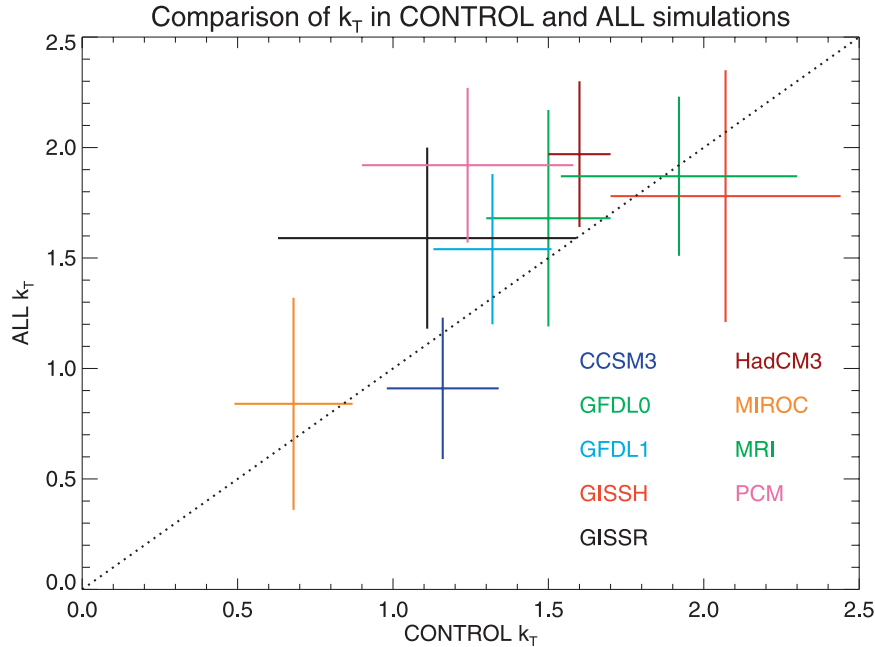
FIG. 6. Values of global mean k_T in the ALL and control simulation comparison. The crosses represent 10%–90% confidence intervals for each model. If forced and unforced variations in surface temperature produce the same k_T, then we would expect the crosses to lie along the dotted line, $y = x$.

trend in all the models that is dependent on the differing responses of precipitation to ΔF_C and ΔF_S takes over. We find $k_T = 1.04 \pm 0.84$ W m^{-2} K^{-1}, $\beta_C = -0.45 \pm 0.34$, and $\beta_S = 0.28 \pm 0.33$.

The model mean is not a good representation of the observed precipitation. Lambert et al. (2005) found that although five of the nine GCMs we consider here adequately represent the response of land-mean precipitation to SARF, the model mean does not. As expected, then, we find that the observed land precipitation change cannot be explained using the energy budget model and observed land temperatures: $k_T = -2.17 \pm 1.13$ W m^{-2} K^{-1}, $\beta_C = 1.57 \pm 0.46$, and $\beta_S = 1.91 \pm 0.49$. All three parameter values are apparently unphysical and the fit to the observations is very poor; see Fig. 5c. These results were obtained using the means of

ΔF_C and ΔF_S across models. Similarly unsatisfactory numbers are found using other estimates of SARF.

d. GCM global-mean precipitation using MIROC SPRINTARS absorption data

We now employ the MIROC SPRINTARS absorption data and Eq. (4) for global-mean GCM precipitation. We find values of k_T that are consistent with those calculated in section 4a, although that for MIROC is somewhat larger here; see Table 4. Values of β_{AC} are satisfactory, being negative and > -1 or small and consistent with zero. Apart from in PCM, values of β_{AC} are consistent with the values of β_C calculated above, which is not surprising when we consider that the total GHG and black carbon SARF absorption is similar to the total black carbon and GHG SARF (Fig. 3a).

TABLE 3. Regression coefficients for global means when values of the global-mean control k_T from Table 2 are imposed on the regression. Values of β_C and β_S and their confidence limits are given for the forced ensemble means for 1913–97. The F-test P value is quoted as a consistency check on residual variance. Values in boldface are significant at the 10% level.

	CCSM3	GFDL0	GFDL1	GISSH	GISSR	HadCM3	MIROC	MRI	PCM
β_C	0.07	**−0.35**	**−0.42**	**−0.32**	**−0.16**	**−0.12**	**−0.21**	**−0.13**	**0.10**
10%–90%	0.07	**0.06**	**0.06**	**0.08**	**0.05**	**0.07**	**0.08**	**0.05**	**0.07**
β_S	**0.28**	**0.20**	0.00	**0.28**	**0.36**	**0.12**	**0.29**	**0.16**	**0.47**
10%–90%	**0.09**	**0.14**	0.12	**0.11**	**0.06**	**0.07**	**0.10**	**0.09**	**0.10**
F test	1.00	**0.35**	**0.57**	0.91	0.96	**0.81**	0.98	1.00	0.97

TABLE 4. Regression coefficients for global means when MIROC SPRINTARS SARF absorption data are used instead of SARF data. Control run values of k_T are the same as in Table 2. Values of k_T, β_{AC}, and β_{AS} and their confidence limits are then given for the forced ensemble means for 1913–97. The F-test P value is quoted as a consistency check on the residual variance. Values in boldface are significant at the 10% level.

	CCSM3	GFDL0	GFDL1	GISSH	GISSR	HadCM3	MIROC	MRI	PCM
k_T (W m^{-2} K^{-1})	**1.22**	**1.76**	**1.63**	**2.41**	**2.12**	**2.17**	**1.52**	**1.54**	**2.10**
10%–90%	0.32	0.55	0.40	0.40	0.28	0.33	0.45	0.47	0.40
β_{AC}	−0.08	**−0.40**	**−0.44**	**−0.45**	**−0.48**	**−0.47**	**−0.43**	−0.04	**−0.45**
10%–90%	0.09	0.12	0.08	0.06	0.05	0.15	0.07	0.25	0.18
β_{AS}	**0.87**	0.79	−0.21	**1.03**	**0.57**	0.34	0.02	**1.06**	**1.52**
10%–90%	**0.41**	0.91	0.85	**0.47**	**0.31**	0.44	0.47	**0.53**	**0.62**
F test	1.00	**0.23**	**0.48**	**0.75**	**0.89**	**0.71**	**0.80**	1.00	**0.75**

Values of β_{AS} are not as we expect, being large and positive in five cases. This problem may be connected with using absorption data from one model, as β_{AS} is small and consistent with zero in MIROC. In mitigation, we note that the total size of the $\beta_{AS} \Delta A_S$ terms is small compared with the $\beta_S \Delta F_S$ terms, because ΔA_S is small compared with ΔF_S (Figs. 3c and 3d). (The correlation between the annual-mean ΔF_S and the annual-mean ΔA_S across the models is 0.84.) Scaling the black carbon absorption by an order of magnitude, as was done for black carbon SARF in section 4a, causes β_{AC} to tend to zero as the scaling factor tends to 10. Hence, the overall size of $\beta_{AC} \Delta A_C$ is little affected. Importantly, there are no significant changes to k_T or β_{AS}.

Despite the good fit for MIROC with global data, using the absorption data does not help us fit the energy budget model to land-only data.

5. Land–atmosphere coupling

What constrains the precipitation change over land? In the previous section, we found that including a land–ocean energy transport term in our energy budget argument does not help. One of the most obvious differences between land and ocean is the effectively limitless availability of moisture over the ocean. Over land, meanwhile, it has been shown that changes in soil moisture content can have a significant effect on precipitation in GCMs. Koster et al. (2004) identified large regions in the Northern Hemisphere during summer in which soil moisture exerted an influence on precipitation change in 16 GCMs. In such "moisture limited" environments, soil moisture controls the tendency of the atmosphere to produce precipitation through its impacts on tropospheric boundary layer humidity and the near-surface energy budget, particularly during the summer (Schär et al. 1999). [It is not the case, however, that local evaporation must provide the bulk of local rainfall; see McDonald (1962).] This does not necessarily mean that global land-mean precipitation is changed by regional links between soil moisture and precipitation, though, because there could be compensating changes in rainfall elsewhere.

In our GCMs, we find temperature-dependent soil moisture decreases in similar regions to those identified as showing large soil moisture–precipitation coupling by Koster et al. (2004); see Fig. 7. (Having said this, some of these regions show opposing changes in soil moisture and near-surface atmospheric relative humidity.) So far, studies of the link between soil moisture and land precipitation have focused on the predictability of regional precipitation (e.g., Dirmeyer (2006)) or on idealized GCM experiments (e.g., Schär et al. 1999; Koster et al. 2004). We believe that an investigation into the effects of land–atmosphere coupling during the entire twentieth century may give some insight into why land and ocean precipitation changes differ so much while land and ocean temperature changes do not.

6. Differing responses of twentieth- and twenty-first-century precipitation

Held and Soden (2006) compared precipitation increases per degree global warming in twentieth-century and IPCC Special Report on Emissions Scenarios (SRES) scenario A1B twenty-first-century GCM runs. [The SRES A1B scenario is a strongly GHG forced future taken from Nakicenovic et al. (2000).] They found that precipitation increased by about 2% K^{-1} across the models, but that twentieth-century values have a mean offset of −1% for all ΔT. Held and Soden (2006) attributed this to the temperature-independent effects of absorbing aerosols, which are a relatively larger proportion of twentieth-century SARF than A1B twenty-first-century SARF. In our language, their hypothesis is that β_C is more negative for black carbon aerosol SARF than GHG SARF. Our methodology cannot estimate the relative sizes of β_C for black carbon and GHGs, as the SARF time series are well correlated (Fig. 3). In section 4d, however, we experimented with increasing
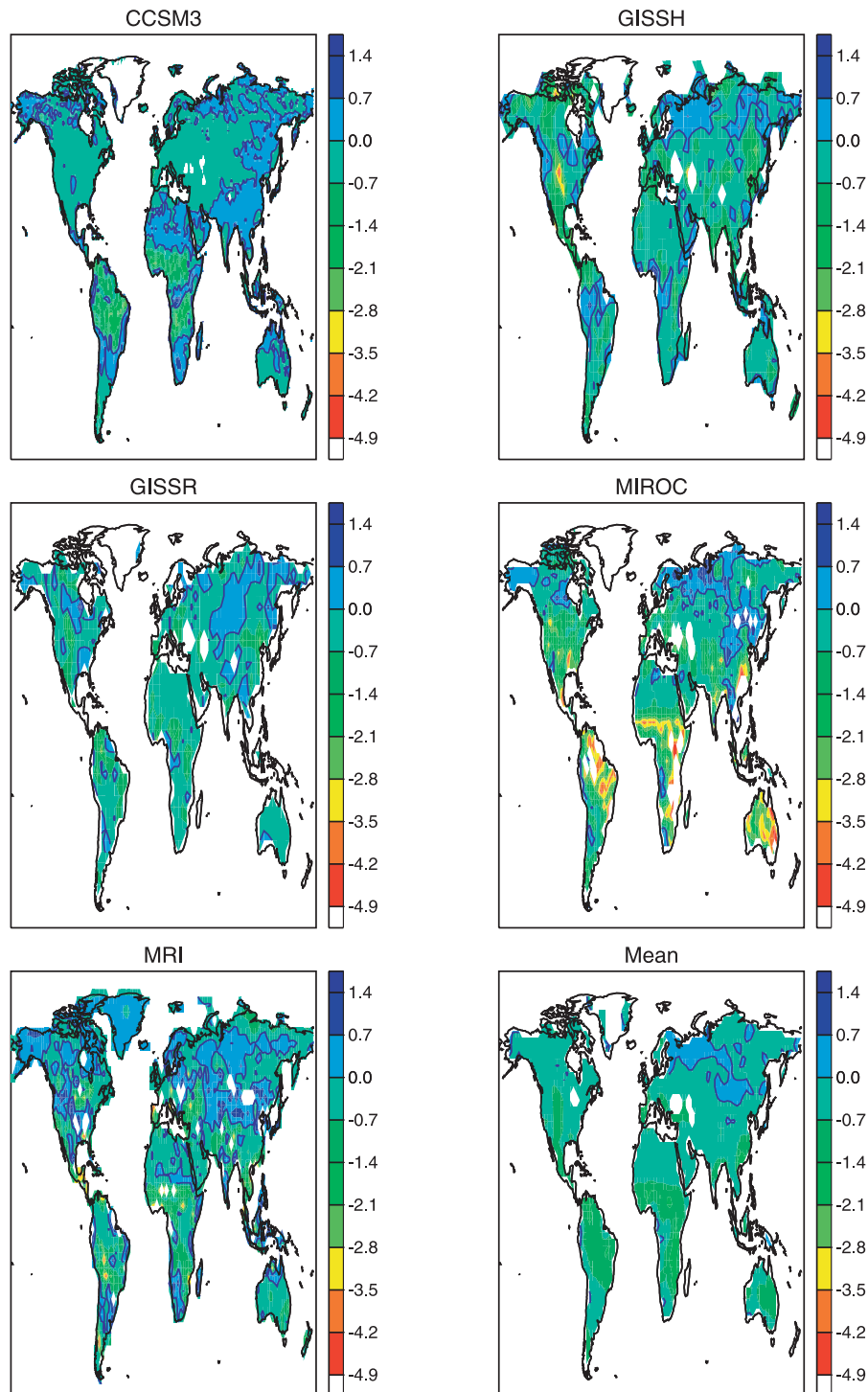
FIG. 7. Trends in soil moisture in the upper 0.1 m of the land surface in kg m^{-2} K^{-1} for 1913–97 in five models for which we have data, and for the model mean giving equal weight to each model. The solid dark-blue lines indicate zero change. The trends are calculated as gridbox soil moisture per degree gridbox warming.

TABLE 5. Values of ensemble-mean twentieth-century and A1B twenty-first-century precipitation changes calculated from Held and Soden's (HS) method compared to values calculated from Eq. (5). The errors are 10%–90% confidence limits for the Eq. (5) values.

	CCSM3	GFDL0	GFDL1	GISSH	GISSR	HadCM3	MIROC	MRI	PCM
HS twentieth (% K^{-1})	1.22	−0.02	−0.04	−0.70	−0.73	1.13	−1.64	1.87	1.39
Eq. (5) (% K^{-1})	1.07	0.02	−0.22	−0.67	−0.78	1.20	−1.51	1.98	1.24
10%–90%	0.67	0.93	0.64	1.50	1.03	0.67	1.25	0.71	0.63
HS twenty-first (% K^{-1})	2.45	0.87	0.98	1.83	1.97	1.00	1.66	2.44	1.71
Eq. (5) (% K^{-1})	1.62	1.43	0.81	1.65	1.17	1.96	0.76	2.37	1.95
10%–90%	0.50	0.66	0.47	0.81	0.60	0.44	0.67	0.59	0.53

the magnitude of the temperature-independent effect of black carbon by as much as a factor of 10. This only tended to reduce our best estimates of β_{AC} toward zero. Hence, we cannot produce the kind of behavior that Held and Soden (2006) suggest with our regression model. This does not mean that it cannot happen, of course. In HadCM3, which is not forced by black carbon (Table 1), the increase in percent per degree kelvin precipitation change seen in the other GCMs during the twenty-first century does not occur (Table 5). MRI and PCM, on the other hand, which are also not forced by black carbon (Table 1), still produce twenty-first-century precipitation changes around 25% larger per degree warming than twentieth-century changes.

An alternative explanation is that anthropogenic sulfate aerosols, which, like black carbon, are a larger fraction of twentieth-century SARF compared with twenty-first-century SARF, are responsible. If sulfates have a negligible direct effect on precipitation ($\beta_S \sim 0$), then sulfate-driven cooling during the twentieth century will tend to reduce precipitation more strongly than GHG- and black-carbon-driven warming increases it per unit SARF.

To investigate this, we repeat the analysis of Held and Soden (2006) by taking the difference between the first and last 20 yr for both our twentieth-century and A1B ensemble means. We compare these results to those found using the energy budget argument, by expressing Eq. (3) in percent per degree kelvin by dividing through by $LP_{clim}\Delta T$, where P_{clim} is the 1961–90 precipitation climatology against which the percentage change is calculated. We obtain

$$\frac{\Delta P}{P_{clim}\Delta T} \simeq \frac{k_T}{LP_{clim}} + \frac{\beta_C \Delta F_C}{LP_{clim}\Delta T} + \frac{\beta_S \Delta F_S}{LP_{clim}\Delta T}. \quad (5)$$

We then substitute GCM twentieth- and twenty-first-century ΔT and twentieth-century and SRES A1B SARF into Eq. (5) and calculate the change expected when we use the parameters fitted in section 4a. The results are presented in Table 5.

The percent per degree kelvin changes calculated from Eq. (5) agree well with Held and Soden–type values for the twentieth century. This is not surprising, since the regression model was trained on these data, albeit using 5-yr means. Agreement during the twenty-first century is fairly good for most models, although the values for CCSM3, GISS (E-R), HadCM3, and MIROC are significantly in error, even though the 10%–90% ranges are large. In particular, Eq. (5) fails to predict the small decrease in precipitation sensitivity shown by HadCM3 during the twenty-first century. The failure may be due to the paucity of training data, although we would expect this to manifest itself through very large error bars. Alternatively, Eq. (5) fitted to twentieth-century data may not fully capture the physical processes behind twenty-first-century precipitation changes— perhaps because k_T depends on time scale, climate state, or forcing type (see section 7).

Still, our results indicate that the relative contributions of GHGs and sulfate aerosols to total SARF may play a role in determining the percent per degree kelvin changes in precipitation. The concept of precipitation sensitivity to global warming can be misleading, because the forcing scenario under consideration is important.

7. Discussion

Changes in GCM twentieth-century global-mean and ocean-mean precipitation can be described by a simple model of the perturbation energy budget of the troposphere. In the nine GCMs we consider, increases in tropospheric temperature that increase tropospheric cooling produce increases in precipitation. When the warming is due to GHG SARF, the direct effect of GHGs on the troposphere causes significant decreases in tropospheric cooling unrelated to temperature, reducing the overall effect of GHGs on precipitation. As a result, precipitation responds more strongly to solar and sulfate aerosol SARF per unit temperature than it does to GHG SARF (Mitchell et al. 1987; Allen and Ingram 2002; Yang et al. 2003). Precipitation changes to different degrees in different GCMs but can be fitted to a linear equation with three parameters. The largest problem with the global-mean results is an apparent

significant and positive temperature-independent effect of reflecting sulfate aerosol and solar SARF on precipitation in five of the nine models. This may be an artifact of the regression analysis. It may also be a gap in our physical understanding. Residual consistency tests also suggest that the energy budget model does not fully account for forced changes in precipitation. However, agreement between energy budget model precipitation and the nine-GCM mean looks excellent; see Figs. 5a and 5b.

Fitting the energy budget model to twentieth-century GCM data allows us to predict twentieth- and twenty-first-century percent per degree kelvin changes in precipitation. Unsurprisingly, the energy budget model competently predicts all-century twentieth-century GCM precipitation changes, because this is the period upon which the model is trained. It also predicts twenty-first-century precipitation changes that are consistent with those found in five of the nine GCMs, although the energy budget model error bars are considerable. Only HadCM3 shows a smaller precipitation sensitivity per degree warming during the twenty-first century, which is not anticipated by our model and is possibly related to nonsimulation of the effects of absorbing black carbon aerosols (Held and Soden 2006). However, the MRI and PCM models also do not simulate black carbon and show greater precipitation sensitivities in the twenty-first century.

On the whole, the nature of global precipitation change is qualitatively consistent with our understanding of the troposphere. Estimates of the effect of increasing temperature on precipitation are robust against considering SARF absorbed by the troposphere, ΔA, as opposed to SARF itself, ΔF. Both surface-temperature-dependent and GHG surface-temperature-independent effects are consistent with those found in the idealized GCM experiments of Lambert and Faull (2007). The direct effects of solar shortwave and sulfate aerosols, on the other hand, are very uncertain, apparently taking the wrong sign in some cases.

In common with earlier work, we have assumed that k_T, the constant of proportionality between the global-mean surface temperature and dependent changes in global-mean precipitation, is the same for different forcings. Only the Lambert and Faull (2007) experiments provide direct support for this, and only for CO_2 and solar forcings. In this paper, we additionally find that surface-temperature-driven changes in precipitation due to natural variability mostly follow the same k_T as forced changes. Nevertheless, it would be useful to have idealized experiments for a range of forcings. We have also not considered the possibility that oceanic adjustment could impact on k_T. Williams et al. (2008)

have shown that changes in ocean properties cause changes in temperature climate sensitivity to radiative forcing on time scales of a few decades. Given that these not only affect patterns of surface temperature change, but also atmospheric lapse rates, moisture, and clouds, there could be significant effects on k_T. A future investigation of this might explain why the energy budget model sometimes fails to predict changes in twenty-first-century precipitation.

Over land, our linear perturbation energy budget equation does not constrain precipitation. Adding a land–sea atmospheric heat transport term to the regression does not solve the problem in five GCMs for which we have heat transport data. Land precipitation may not be explicable using a linear equation and the approximations that we employ. We note that the average behavior across all nine GCMs can be described using the energy budget, and that average land precipitation does respond more strongly to shortwave SARF per unit temperature. This is not a physical explanation, however, as the average does not describe land precipitation changes in the observations or most individual GCMs. Land surface processes may cause different changes in precipitation in different models. Based on our results, and those of Koster et al. (2004), it may be that the availability of soil moisture is important. There could also be significant differences in SARF between land and ocean. Land–ocean heat fluxes may still play a role that is indiscernible with a linear model. These two factors could be particularly important under the rapid changes in SARF caused by volcanic eruptions.

Is the energy budget picture of precipitation useful? We reach the unhappy conclusion that we cannot explain precipitation changes over land, where we have good observations, but may broadly understand precipitation changes over the oceans, where we have no observations. Clearly, a probabilistic forecast of twenty-first-century land precipitation of the form of Stott and Kettleborough (2002) based on observations is not possible. However, energy conservation probably does explain why twentieth-century land precipitation has been dominated by changes in volcanic shortwave SARF, as was found by Gillett et al. (2004). It also gives us strong reasons to believe that changes in oceanic precipitation do not follow the Clausius–Clapeyron equation even if changes in atmospheric moisture do ($\sim 7.5\%$ K^{-1}). [The same is not true of extreme precipitation, however; see Pall et al. (2007).] This remains the case, even though Wentz et al. (2007) found that global precipitation changes during the past 20 yr are consistent with moisture changes. Wentz's results not only neglect natural variability, but also a possible large increase in recent $\beta_S \Delta F_S$ caused by recent decreases in

atmospheric aerosol concentration (Romanou et al. 2007). This decrease, termed global brightening, is not included in the majority of the contemporary GCM simulations and may provide an explanation for the large precipitation increases since the 1980s. Indeed, Previdi and Liepert (2008) have shown that GCMs can produce changes of 7% K^{-1} or even more during 20-yr periods. Finally, the energy budget approach urges caution in basing predictions of twenty-first-century precipitation on the response of twentieth-century precipitation to temperature. This is likely to be important if twenty-first-century SARF is dominated by GHG longwave SARF.

REFERENCES

Allen, M. R., and W. J. Ingram, 2002: Constraints on future changes in climate and the hydrologic cycle. *Nature,* **419,** 224–232.

Boer, G. J., 1993: Climate change and the regulation of the surface moisture and energy budgets. *Climate Dyn.,* **8,** 225–239.

Brohan, P., J. J. Kennedy, I. Harris, S. F. B. Tett, and P. D. Jones, 2006: Uncertainty estimates in regional and global observed temperature changes: A new data set from 1850. *J. Geophys. Res.,* **111,** D12106, doi:10.1029/2005JD006548.

Collins, W. D., and Coauthors, 2006: Radiative forcing by well-mixed greenhouse gases: Estimates from climate models in the Intergovernmental Panel on Climate Change (IPCC) Fourth Assessment Report (AR4). *J. Geophys. Res.,* **111,** D14317, doi:10.1029/2005JD006713.

Dirmeyer, P. A., 2006: The hydrologic feedback pathway for land–climate coupling. *J. Hydrometeor.,* **7,** 857–867.

Douville, H., D. Salas-Mèlia, and S. Tyteca, 2006: On the tropical origin of uncertainties in the global land precipitation response to global warming. *Climate Dyn.,* **26,** 367–385.

Gillett, N. P., A. J. Weaver, F. W. Zwiers, and M. F. Wehner, 2004: Detection of volcanic influence on global precipitation. *Geophys. Res. Lett.,* **31,** L12217, doi:10.1029/2004GL020044.

Goody, R. M., and Y. L. Yung, 1989: *Atmospheric Radiation: Theoretical Basis.* 2nd ed. Oxford University Press, 519 pp.

Gordon, C., C. Cooper, C. A. Senior, H. Banks, J. M. Gregory, T. C. Johns, J. F. B. Mitchell, and R. A. Wood, 2000: The simulation of SST, sea ice extents and ocean heat transports in a version of the Hadley Centre coupled model without flux adjustments. *Climate Dyn.,* **16,** 147–168.

Gregory, J. M., and M. J. Webb, 2008: Tropospheric adjustment induces a cloud component in CO_2 forcing. *J. Climate,* **21,** 58–71.

——, and Coauthors, 2004: A new method for diagnosing radiative forcing and climate sensitivity. *Geophys. Res. Lett.,* **31,** L03205, doi:10.1029/2003GL018747.

Hansen, J. E., and M. Sato, 2001: Trends of measured climate forcing agents. *Proc. Natl. Acad. Sci. USA,* **98,** 14 778–14 783, doi:10.1073/pnas.261553698.

Haywood, J. M., D. L. Roberts, A. Slingo, J. M. Edwards, and K. P. Shine, 1997: General circulation model calculations of the direct radiative forcing by anthropogenic sulfate and fossil-fuel soot aerosol. *J. Climate,* **10,** 1562–1577.

Held, I. M., and B. J. Soden, 2006: Robust responses of the hydrological cycle to global warming. *J. Climate,* **19,** 5686–5699.

Hoyt, D., and K. H. Schatten, 1993: A discussion of plausible solar irradiance variations, 1700–1992. *J. Geophys. Res.,* **98,** 18 895–18 906.

Huffman, G. J., and Coauthors, 1997: The Global Precipitation Climatology Project (GPCP) Combined Precipitation Dataset. *Bull. Amer. Meteor. Soc.,* **78,** 5–20.

Hulme, M., 1992: A 1951–80 global land precipitation climatology for the evaluation of general circulation models. *Climate Dyn.,* **7,** 57–72.

James, I. N., 1994: *Introduction to Circulating Atmospheres.* Cambridge University Press, 422 pp.

Johns, T. C., and Coauthors, 2003: Anthropogenic climate change for 1860 to 2100 simulated with the HadCM3 model under updated emissions scenarios. *Climate Dyn.,* **20,** 583–612.

Koster, R. D., and Coauthors, 2004: Regions of strong coupling between soil moisture and precipitation. *Science,* **305,** 1138–1140.

Lambert, F. H., and N. E. Faull, 2007: Tropospheric adjustment: The response of two general circulation models to a change in insolation. *Geophys. Res. Lett.,* **34,** L03701, doi:10.1029/2006GL028124.

——, P. A. Stott, M. R. Allen, and M. A. Palmer, 2004: Detection and attribution of changes in 20th century land precipitation. *Geophys. Res. Lett.,* **31,** L10203, doi:10.1029/2004GL019545.

——, N. P. Gillett, D. A. Stone, and C. Huntingford, 2005: Attribution studies of observed land precipitation changes with nine coupled models. *Geophys. Res. Lett.,* **32,** L18704, doi:10.1029/2005GL023654.

Lean, J. L., J. Beer, and R. Bradley, 1995: Reconstruction of solar irradiance since 1610: Implications for climate change. *Geophys. Res. Lett.,* **22,** 3195–3198.

——, Y. Wang, and N. R. Sheeley Jr., 2002: The effect of increasing solar activity on the sun's total and open magnetic flux during multiple cycles: Implications for solar forcing of climate. *Geophys. Res. Lett.,* **29,** 2224, doi:10.1029/2002GL015880.

Liepert, B. G., J. Feichter, U. Lohmann, and E. Roeckner, 2004: Can aerosols spin down the water cycle in a warmer and moister world? *Geophys. Res. Lett.,* **31,** L06207, doi:10.1029/2003GL019060.

McDonald, J. E., 1962: The evaporation–precipitation fallacy. *Weather,* **17,** 168–177.

Menon, S., V. K. Saxena, P. D. B. N. Wenny, and K. Nielsen, 2002: Role of sulfate aerosols in modifying the cloud albedo: A closure experiment. *Atmos. Res.,* **61,** 169–187.

Mitchell, J. F. B., C. A. Wilson, and W. M. Cunnington, 1987: On CO_2 climate sensitivity and model dependence of results. *Quart. J. Roy. Meteor. Soc.,* **113,** 293–322.

Nakicenovic, N., and Coauthors, 2000: *IPCC Special Report on Emissions Scenarios.* Cambridge University Press, 612 pp.

New, M., M. Hulme, and P. Jones, 2000: Representing twentieth-century space–time climate variability. Part II: Development of 1901–96 monthly grids of terrestrial surface climate. *J. Climate,* **13,** 2217–2238.

Pall, P., M. R. Allen, and D. A. Stone, 2007: Testing the Clausius–Clapeyron constraint on changes in extreme precipitation under CO_2 warming. *Climate Dyn.,* **28,** 351–363.

Previdi, M., and B. Liepert, 2008: Monitoring and understanding rainfall changes on a warming planet. *Eos, Trans. Amer. Geophys. Union,* **89,** 193, doi:10.1029/2008EO210002.

Ramachandran, S., V. Ramaswamy, G. L. Stenchikov, and A. Robock, 2000: Radiative impacts of the Mt. Pinatubo volcanic eruption: Lower stratospheric response. *J. Geophys. Res.,* **105,** 409–424.

Ramanathan, V., P. J. Crutzen, J. T. Kiehl, and D. Rosenfeld, 2001: Aerosols, climate, and the hydrological cycle. *Science,* **294,** 2119–2124.

Roberts, D. L., and A. Jones, 2004: Climate sensitivity to black carbon aerosol from fossil fuel combustion. *J. Geophys. Res.,* **109,** D16202, doi:10.1029/2004JD004676.

Roeckner, E., L. Bengtsson, J. Feichter, J. Lelieveld, and H. Rodhe, 1999: Transient climate change simulations with a coupled atmosphere–ocean GCM including the tropospheric sulfur cycle. *J. Climate,* **12,** 3004–3032.

Romanou, A., B. Liepert, G. A. Schmidt, W. B. Rossow, R. A. Ruedy, and Y. Zhang, 2007: 20th century changes in surface solar irradiance in simulations and observations. *Geophys. Res. Lett.,* **34,** L05713, doi:10.1029/2006GL028356.

Rotstayn, L. D., and J. E. Penner, 2001: Indirect aerosol forcing, quasi forcing, and climate response. *J. Climate,* **14,** 2960–2975.

Sato, M., J. E. Hansen, M. P. McCormick, and J. B. Pollack, 1993: Stratospheric aerosol optical depth, 1850–1990. *J. Geophys. Res.,* **98,** 22 987–22 994.

Schär, C., D. Lüthi, and U. Beyerle, 1999: The soil–precipitation feedback: A process study with a regional climate model. *J. Climate,* **12,** 722–741.

Shine, K. P., J. Cook, E. J. Highwood, and M. M. Joshi, 2003: An alternative to radiative forcing for estimating the relative importance of climate change mechanisms. *Geophys. Res. Lett.,* **30,** 2047, doi:10.1029/2003GL018141.

Soden, B. J., and I. M. Held, 2006: An assessment of climate feedbacks in coupled ocean–atmosphere models. *J. Climate,* **19,** 3354–3360.

Stott, P. A., and J. A. Kettleborough, 2002: Origins and estimates of uncertainty in predictions of twenty-first century temperature rise. *Nature,* **416,** 723–726.

Takemura, T., Y. Tsushima, T. Yokohata, T. Nazawa, T. Nagashima, and T. Nakajima, 2006: Time evolutions of various radiative forcings for the past 150 years estimated by a general circulation model. *Geophys. Res. Lett.,* **33,** L19705, doi:10.1029/2006GL026666.

Webb, M. J., and Coauthors, 2006: On the contribution of local feedback mechanisms to the range of climate sensitivity in two GCM ensembles. *Climate Dyn.,* **27,** 17–38.

Wentz, F. J., L. Ricciardulli, K. Hilburn, and C. Mears, 2007: How much more rain will global warming bring? *Science,* **317,** 233–235, doi:10.1126/science.ll40746.

Williams, K. D., W. J. Ingram, and J. M. Gregory, 2008: Time variation of effective climate sensitivity in GCMs. *J. Climate,* **21,** 5076–5090.

Xie, P., and P. A. Arkin, 1997: Global precipitation: A 17-year monthly analysis based on gauge observations, satellite estimates, and numerical model outputs. *Bull. Amer. Meteor. Soc.,* **78,** 2539–2558.

Yang, F., A. Kumar, M. E. Schlesinger, and W. Wang, 2003: Intensity of hydrological cycles in warmer climates. *J. Climate,* **16,** 2419–2423.